

ORIGINAL ARTICLE

Open Access



Decoding MRI-informed brain age using mutual information

Jing Li^{1*}, Linda Chiu Wa Lam¹ and Hanna Lu^{1,2*} 

Abstract

Objective We aimed to develop a standardized method to investigate the relationship between estimated brain age and regional morphometric features, meeting the criteria for simplicity, generalization, and intuitive interpretability.

Methods We utilized T1-weighted magnetic resonance imaging (MRI) data from the Cambridge Centre for Ageing and Neuroscience project ($N = 609$) and employed a support vector regression method to train a brain age model. The pre-trained brain age model was applied to the dataset of the brain development project ($N = 547$). Kraskov (KSG) estimator was used to compute the mutual information (MI) value between brain age and regional morphometric features, including gray matter volume (GMV), white matter volume (WMV), cerebrospinal fluid (CSF) volume, and cortical thickness (CT).

Results Among four types of brain features, GMV had the highest MI value (8.71), peaking in the pre-central gyrus (0.69). CSF volume was ranked second (7.76), with the highest MI value in the cingulate (0.87). CT was ranked third (6.22), with the highest MI value in superior temporal gyrus (0.53). WMV had the lowest MI value (4.59), with the insula showing the highest MI value (0.53). For brain parenchyma, the volume of the superior frontal gyrus exhibited the highest MI value (0.80).

Conclusion This is the first demonstration that MI value between estimated brain age and morphometric features may serve as a benchmark for assessing the regional contributions to estimated brain age. Our findings highlighted that both GMV and CSF are the key features that determined the estimated brain age, which may add value to existing computational models of brain age.

Critical relevance statement Mutual information (MI) analysis reveals gray matter volume (GMV) and cerebrospinal fluid (CSF) volume as pivotal in computing individuals' brain age.

Key Points

- Mutual information (MI) interprets estimated brain age with morphometric features.
- Gray matter volume in the pre-central gyrus has the highest MI value for estimated brain age.
- Cerebrospinal fluid volume in the cingulate has the highest MI value.
- Regarding brain parenchymal volume, the superior frontal gyrus has the highest MI value.
- The value of mutual information underscores the key brain regions related to brain age.

Keywords Brain age, Structural MRI, Mutual information, Machine learning, Gray matter volume

*Correspondence:

Jing Li

ljing@link.cuhk.edu.hk

Hanna Lu

hannalu@cuhk.edu.hk

¹Department of Psychiatry, The Chinese University of Hong Kong, Hong Kong SAR, China

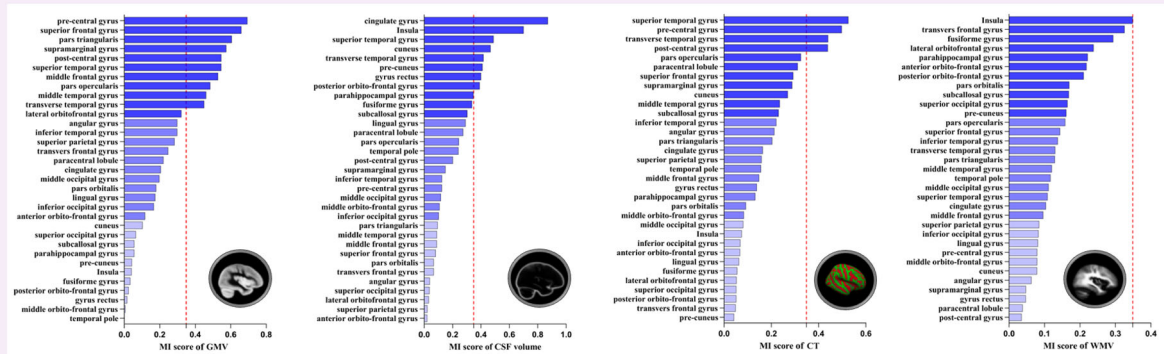
²The Affiliated Brain Hospital of Guangzhou Medical University, Guangzhou, China



© The Author(s) 2024. **Open Access** This article is licensed under a Creative Commons Attribution 4.0 International License, which permits use, sharing, adaptation, distribution and reproduction in any medium or format, as long as you give appropriate credit to the original author(s) and the source, provide a link to the Creative Commons licence, and indicate if changes were made. The images or other third party material in this article are included in the article's Creative Commons licence, unless indicated otherwise in a credit line to the material. If material is not included in the article's Creative Commons licence and your intended use is not permitted by statutory regulation or exceeds the permitted use, you will need to obtain permission directly from the copyright holder. To view a copy of this licence, visit <http://creativecommons.org/licenses/by/4.0/>.

Graphical Abstract

Decoding MRI-informed brain age using mutual information



We employed mutual information (MI) as a benchmark to investigate the relationship between estimated brain age and brain morphometric features, aiming to enhance the interpretability of brain age modes.



**Insights Imaging (2024) Li J, Lam LCW, Lu H.
DOI: 10.1186/s13244-024-01791-9**

Introduction

Aging, as an inevitable and irreversible process, manifests uniquely in each individual and is influenced by a complex interplay of genetic predisposition [1, 2], environmental determinants [3], lifestyle choices [1], and neural plasticity [2]. As individuals progress through the chronological trajectory of life, their brains undergo a series of intricate changes. These brain changes encompass a wide spectrum of physiological and pathological processes, ranging from subtle modifications in cortical layers to region-specific volumetric variations [3, 4], culminating in distinctive patterns of age-related brain morphometry. The structural changes in the brain manifest in a multidimensional manner, impacting both volumetric and surface-based features [5].

With the development of quantitative approaches in neuroimaging, the concept of brain age has been developed for thoroughly estimating an individual's chronological age at individual level [6]. Structural magnetic resonance imaging (sMRI) plays a pivotal role in capturing the subtle yet crucial changes in brain morphometry that unfold over an individual's lifespan. The utilization of sMRI combined with advanced computational techniques, such as machine learning algorithms, empowers neuroscientists to develop predictive models linking brain

structures with chronological age [7]. Estimated brain age has the potential to identify deviations from the norms, shedding light on understanding accelerated or decelerated brain aging trajectories [8]. The difference between predicted brain age and chronological age is referred to as the score of brain-PAD (brain-predicted age difference) [9]. For example, when considering an individual with a chronological age of 60 years and a predicted brain of 65 years, the score of brain-PAD is +5 years, indicating that the individual's brain is undergoing an accelerated aging process of +5 years.

The brain age model has shown promising utilities in clinical populations. For example, brain age prediction can be used to identify abnormal aging-related deviations in individuals with psychiatric and neurological disorders, such as schizophrenia and Alzheimer's disease [10–14]. Of note, these deviations from normal aging trajectory can be detected before clinical symptoms appear, allowing for earlier intervention and potentially improving clinical outcomes [7, 13–15]. The estimated brain age may also serve as a biomarker of an individual's brain health during aging [7]. By estimating an individual's brain age, clinicians can gain insights into their cognitive health and the risk of developing age-related conditions [12, 15, 16].

Despite the promise of brain age, it encounters challenges, notably two ‘black boxes’. First, the value of brain age is overly a ‘black box’ [7]. Brain age, estimated from structural brain scans, aggregates the complexities underlying multidimensional alteration patterns of brain aging into one value [16]. Age-related alterations in the brain are subtle, nonlinear, and spatially distributed [17–19]. Although brain age has been widely studied in psychiatric and neurological disorders, the specific features used to predict brain age remain unclear, which may result in disregarding important neuroscientific information [7]. This is of particular concern for researchers to extend the utilities of brain age to conditions whose pathoanatomical deviations from typical aging may feature both global and regional changes. Second, brain age is estimated by utilizing various statistical models, including classical statistical models (e.g., multivariate and univariate regression, general linear models), machine learning models (ML) (e.g., random forest regression, elastic net regression, relevance vector regression), and deep learning techniques (DL) (e.g., convolutional neural networks) [20–25]. It should be noted that most ML and DL techniques are ‘black boxes’ [26]. Unlike traditional statistical methods, where the parameters and assumptions of the models are explicitly defined, the models computed by ML and DL algorithms are operated by optimizing parameters through iterative processes, resulting in complex decision boundaries that are very challenging to interpret. The specific features or patterns identified by the ML and DL models may not be readily interpretable and understood. The ‘black box’ nature of ML and DL models raises concerns about their reliability and accountability when applied to brain age prediction. The lack of interpretability in these models may limit the applications of brain age in clinical populations.

To address these concerns, we employed mutual information (MI) value as a standardized metric to quantify the distinct contributions of morphometric features to estimated brain age. MI is a fundamental notion in information theory, quantifying the extent to which one random variable holds information about another, which is widely employed to gauge the statistical relatedness of any relationship between variables [27]. This property allows MI value to reliably measure the statistical dependency between variables without being affected by transformations, thereby providing a robust and consistent measure of the relationship between estimated brain age and morphometric features across different representations or coordinate systems. The MI value of individual’s variables also remains invariant under any invertible transformations [28]. Thus, using MI value to gauge the impact of input morphometric features on brain age has three-fold advantages: (1) simplicity in

computation, avoiding resource-intensive procedures, especially when dealing with complex models and large datasets; (2) generalizability well across different types of statistical models by capturing the feature patterns in any model; (3) intuitive interpretability, providing understandable insights with minimal needs for statistical assumptions or domain-specific expertise. In this study, we initially employed volumetric- and surface-based brain regional features as training features to develop a brain age model. Subsequently, we utilized the nearest-neighbor method to compute the MI values between each input feature and the estimated brain age [27, 29]. This approach aimed to bridge the gap in the interpretability of brain age models and facilitate the validation of model predictions, thereby enhancing the credibility of brain age estimation. Furthermore, it may advance our understanding of the relationship between brain aging and macroscopic structural changes in aging populations.

Materials and methods

Participants

The training set ($N = 609$, aged from 18 to 88 years) comprising T1-weighted structural MRI scans was obtained from the Cambridge Centre for Aging and Neuroscience (Cam-CAN) study (<https://www.cam-can.org>) [30]. The testing set ($N = 547$, aged from 20 to 86 years) comprised T1-weighted sMRI data from the Brain development project (IXI) (<https://brain-development.org>). The demographic characteristics of the participants in the two datasets, along with the MRI acquisition parameters, are listed in Table 1. As per local study protocols [30], all participants underwent screening to ensure cognitive health and exclude major psychiatric conditions. The testing set served for both validation of the brain age prediction model and quantification of individual feature contributions to the estimated brain age.

Table 1 The detailed information of Cam-CAN and Brain development project

	Cam-CAN	Brain development project (IXI)
Number of subjects	609	547
Males/females	305/304	243/304
Age mean (SD)	53.2 (18.3)	48.6 (16.5)
Age range	18–88	19.98–86.32
TR (ms)	2250	9.6/9.8
TE (ms)	2.99	4.6/4.6
TI (ms)	900	\
FOV	256 × 240 × 192	\

Cam-CAN Cambridge Centre for Aging and Neuroscience, TR repetition time, TE echo time, TI inversion time, FOV field of view, SD Standard deviation

Pre-processing of sMRI scans

Cortical reconstructions and surface-based morphometry analysis of T1-weighted MRI scans were conducted using BrainSuite 21a (<https://brainsuite.org/>) [31]. BrainSuite is a semi-automatic cortical surface identification integrated package, widely employed in aging research [32, 33]. The pre-processing pipeline encompassed the following steps: (1) cortical surface extraction involves several steps: skull-stripping, tissue classification, gross labeling of brain structures, and modeling the inner and outer boundaries of the cerebral cortex. Notably, image enhancement and pre-processing techniques are applied before the skull-stripping process. An anisotropic diffusion filter is applied to smooth contiguous tissue regions while respecting the edge boundaries between them, enhancing the boundary between the brain and other tissues [34]. A three-dimensional Marr Hildreth edge detector and morphological erosion processing are then utilized to remove the skull and scalp from the image [35, 36]. Image non-uniformities are corrected in the stripped brain, using a parametric tissue measurement model [31]; (2) cortical thickness estimation based on partial volume estimates and anisotropic diffusion equation; (3) surface-constrained volumetric registration to create a mapping to a labeled reference atlas (BCI-DNI) [37] and assign labels to the cortical surface and brain volume; (4) alignment of cortical thickness estimates to atlas space; (5) computation of subject-level features, including gray matter volume (GMV), white matter volume (WMV), cerebrospinal fluid (CSF) volume, and cortical thickness in the pre-defined regions of interest. Visual inspections were performed, and any segmentation errors were manually corrected.

Regional cortical features

We utilized four types of regional morphometric features, including GMV, WMV, CSF volume, and cortical thickness, in total 66, as input features for the brain age model. Given the anatomical asymmetry of the brain, we extracted regional morphometric features from both left and right brain hemispheres [38–40]. A total of 66 cortical regions, covering both hemispheres, were chosen according to the BCI-DNI atlas. To systematically explore the impact of regional morphometric features on estimated brain age, we investigated the combinations of different morphometric features for each cortical region, including 66 regional brain parenchyma volume features, merging the GMV and WMV of each cortical region; and 66 regional intracranial volume features, incorporating the GMV, WMV, and CSF volumes of each cortical region.

Support vector regression model

We utilized support vector regression (SVR), a robust regression model implemented with the scikit-learn library

in Python, widely used for estimating brain age [20, 41–46]. SVR seeks to identify a hyperplane that minimizes deviation from training data, akin to linear regression [47]. Unlike linear regression, SVR could compute errors solely from data points beyond a ‘margin of tolerance’ set by the hyperparameter epsilon (ϵ), known as support vectors, which dictate the hyperplane’s placement. The regularization hyperparameter ‘C’ plays a vital role in striking a balance between hyperplane complexity and training errors, effectively preventing overfitting. We utilized the radial basis function (RBF) kernel to facilitate mapping nonlinear data into higher dimensions through the ‘kernel trick’. We applied a nested 10-fold cross-validation scheme and GridSearchCV function with the ‘neg_mean_absolute_error’ scoring parameter to determine the optimal regularization hyperparameters for SVR. We then used the ‘best_params_’ attribute to obtain the value of the regularization hyperparameter ‘C’, resulting in $C = 1$.

Age-bias correction

In the estimation of brain age, a common phenomenon is age-related bias, with younger individuals often having overestimated brain ages and older individuals having underestimated brain ages due to general statistical features of the regression analysis [41, 48, 49]. To address this age-related bias, we employed a statistical age-bias correction method. This method involves fitting the estimated brain age into a regression function:

$$\text{corrected age}_i = a\hat{\text{age}}_i + [\text{age}_i - (\alpha \times \text{age}_i + \beta)]$$

In this equation, corrected age_i represents the corrected brain age for subject i , $a\hat{\text{age}}_i$ is the first estimated brain age, and age_i is the chronological age of subject i . The correction coefficients α and β are estimated through a fit in the training set and subsequently applied to correct estimations in the testing set [50].

Decoding the contributions of brain regions

Mutual information (MI) gauges the interdependence of variables, first defined and analyzed by Shannon in 1948 [51]. MI is based on the concept of entropy, which measures the uncertainty or randomness of a random variable. The calculation of entropy is based on the probability function of the random variable, where higher entropy indicates greater uncertainty and information. For a random variable, x , its entropy, denoted by $H(x)$, represents the uncertainty associated with x . The entropy of x is:

$$H(x) = - \sum_{i=1}^n p(x(i)) \cdot \log(x(i))$$

$x(i)$ represents each possible outcome of the random variable x . $P(x(i))$ is the marginal probability of $x(i)$. For

two variables, x and y , their MI: $I(x; y)$ quantifies the reduction in uncertainty about one variable when the other variable is known. Mathematically, MI can be expressed as the difference between the joint entropy of x and y , and the sum of their individual entropies:

$$I(x; y) = H(x) + H(y) - H(x, y)$$

$$I(x; y) = \sum_{i=1}^n \sum_{j=1}^n p(x(i), y(j)) \left(\frac{p(x(i), y(j))}{p(x(i)) \cdot p(y(j))} \right)$$

MI is non-negative ($I(x; y) \geq 0$) and symmetric ($I(x; y) = I(y; x)$). A MI value of zero indicates that the two variables are independent, meaning the knowledge of one variable does not provide any information about the other variable. A higher MI value signifies stronger dependencies between variables. In this study, we applied the KSG estimator proposed by Kraskov, Stögbauer, and Grassberger for computing the MI [27]. The KSG method involves an adaptive non-parametric approach that estimates MI without making assumptions about the underlying probability distributions. It utilizes a k -nearest neighbor to estimate local densities and adaptive bin the data. The KSG method offers advantages such as robustness to noise and adaptiveness to data structure. Below is the equation:

$$I(X, Y) = \psi(k) - \langle \psi(n_x + 1) + \psi(n_y + 1) \rangle + \psi(N)$$

N is the number of data points in the joint space.

k is the number of nearest neighbors.

ψ is the digamma function.

n_x and n_y are neighbor counts within X and Y marginal spaces.

Results

Model performance

The brain age model was trained using 264 training features, encompassing mean cortical thickness, regional volumes of GMV, WMV, and CSF. Three commonly used metrics of model performance were included in this study: (1) root-mean-square error (RMSE) [52], (2) mean absolute error (MAE) [52], and (3) coefficient of determination (R^2) [53]. The age-bias correction coefficients ($\alpha = 0.885$, $\beta = 5.658$) were derived from a fit in the training set and applied to correct predictions in the independent testing set. On the training set, the model reached an accuracy of MAE = 5.32 years, RMSE = 6.64 years, and $R^2 = 0.87$. After age-bias correction, the performance of the brain age model was improved accordingly (MAE = 5.15 years, RMSE = 6.27 years and $R^2 = 0.88$).

In the independent testing set, the relationship between chronological age and estimated brain age, as well as

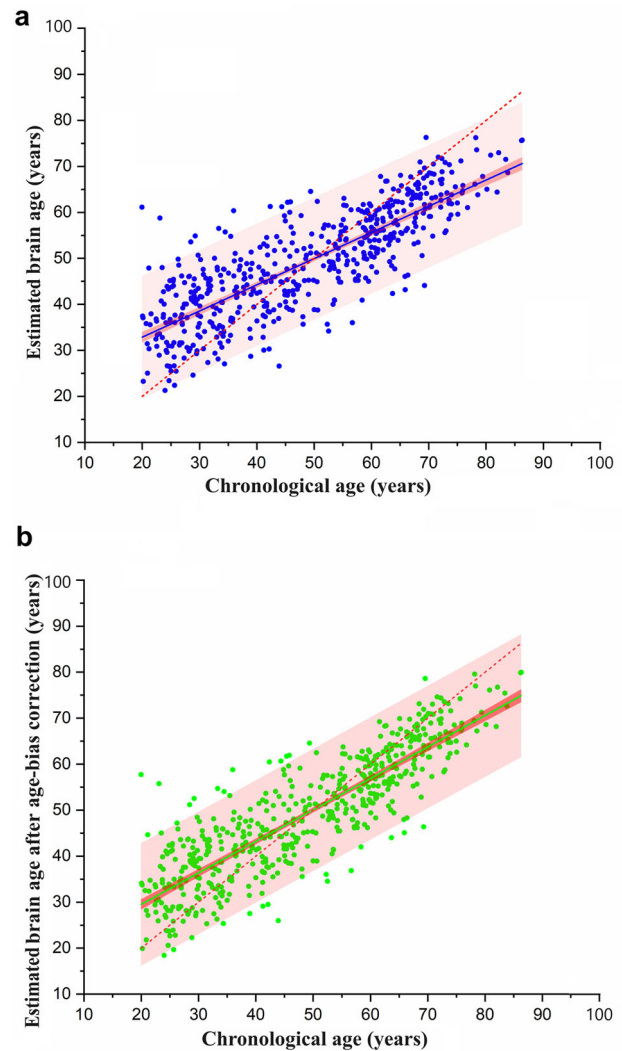


Fig. 1 The relationship between estimated brain age and chronological age in the testing set. Prediction bands and 95% confidence bands are presented. **a** presents the relationship between estimated brain age and chronological age. The red line is a regression line fitted when estimated brain age equals chronological age. The blue line is a regression line fitted between estimated brain age and chronological age. **b** displays the relationship between the estimated brain age after age-bias correction. The red line is a regression line fitted when the age-bias-corrected estimated brain age equals chronological age. The green line is a regression line fitted between the estimated brain age after age-bias correction and chronological age

chronological age and estimated brain age after age-bias correction, were illustrated in Fig. 1. The performance of the brain age model in the testing set had a slight decrease, resulting in MAE = 7.79 years, RMSE = 9.80 years, and $R^2 = 0.66$. However, after age-bias correction, an improvement in the model's prediction accuracy was observed: MAE = 6.65 years, RMSE = 8.53 years, and $R^2 = 0.74$.

Contributions of different brain features

The MI values between the estimated brain age and each input brain feature were computed separately. Furthermore, to explore associations between regional brain parenchyma volumes and estimated brain age, we aggregated the MI values of GMV and WMV within the same brain region. To investigate the relationship between regional intracranial volumes and estimated brain age, we aggregated the MI values of GMV, WMV, and CSF volume within each brain region. Geometric asymmetry between brain hemispheres was considered, with input features from both hemispheres included for each brain region. To focus on the overall morphometric characteristics of brain regions, MI values for the same brain region across the hemispheres were merged. The MI values for the 33 cortical brain regions, shown in Figs. 2–4, with the top ten ranked visualized as heatmaps in Fig. 5.

Notably, although the total MI value (27.28) between age-corrected brain age and all features was lower than the total MI value (28.21) between estimated brain age and all features, there were no significant differences in the MI values between age-corrected brain age, estimated brain age, and the features of each brain region. Given that age-bias correction is a commonly employed step in brain age estimations, we discussed the results obtained from the age-corrected brain age to dissect the specific contributions of brain region features. Among the four types of brain features, GMV exhibited the highest total MI value (8.71), with the pre-central gyrus having the highest MI score (0.69) (Fig. 5a). The second-highest total MI value was associated with CSF volume (7.76), with the cingulate having the highest MI score (0.87) (Fig. 5b). The third-highest total MI value corresponded to mean CT (6.22), with the superior temporal gyrus showing the highest MI value (0.53) (Fig. 5c). WMV had the lowest total MI value (4.59), with the highest MI value observed in the insula (0.35) (Fig. 5d). Regarding the brain parenchymal volume (the combination of GMV and WMV), the superior frontal gyrus exhibited the highest total MI value (0.80) (Fig. 5e). In the case of intracranial total volume (the combination of GMV, WMV, and CSF volume), the cingulate showed the highest total MI value (1.18) (Fig. 5f).

MI in gender-specific testing subgroups

We divided the IXI dataset into female subgroup (sample size: 304; age range: 19.98–86.32 years), and male subgroup (sample size: 243; age range: 20.07–86.20 years). The brain age prediction model performance on the male subgroup is $R^2 = 0.68$, MAE = 7.74 years, and RMSE = 9.61 years. After age-bias correction, the model performance on the male subgroup is slightly improved: $R^2 = 0.75$, MAE = 6.67 years, and RMSE = 8.37 years. The

brain age prediction model on the female subgroup is $R^2 = 0.64$, MAE = 7.84 years, and RMSE = 9.96 years, which is less accurate than on the male subgroup. After age-bias correction, the model performance on the female subgroup is slightly improved: $R^2 = 0.72$, MAE = 6.65 years, and RMSE = 8.66 years. We computed the MI between estimated brain age after age-bias correction and all features in male and female subgroups. The total MI in the male subgroup is 32.65, which is higher than the total MI in the female subgroup (28.58). In the male subgroup, CSF volume exhibited the highest MI (11.62) among the four types of brain features, while GMV exhibited the second-highest MI (8.95). In the female subgroup, GMV exhibited the highest MI (9.78) among the four types of brain features, while CSF volume exhibited the second-highest MI (7.80). We calculated the Spearman ranking correlation coefficient and p -value to assess the statistical significance of MI in brain regions between male and female subgroups, and the whole testing dataset. A significance level of 0.05 was set. The results suggested that there was no significant difference in the MI value rankings of each brain region between the female subgroup, the male subgroup, and the overall testing dataset.

Discussion

In this study, we used four types of morphometric features to train the brain age model. Subsequently, we applied and validated this model to an independent testing dataset to calculate the estimated brain age. Through a comparative analysis of mutual information (MI) values between each input feature, the combinations of input features (brain parenchyma and intracranial total volume), and estimated brain age, we observed several interesting findings. These findings underscore the critical significance of specific MRI-based morphometric features in determining individuals' brain age and providing new insights into the processes of brain aging through computational models. We used gender-specific subgroups to validate our findings, and the results showed that there were no significant differences in the MI value rankings of each brain region among the gender-specific subgroups.

First and foremost, cortical gray matter volume showed the strongest relatedness with estimated brain age. This observation highlights the superior prediction accuracy of brain age models utilizing gray matter as an input feature compared to other types of morphometric features [54, 55], as evidenced by its widespread applications in the research field of brain age [6, 13, 56–61]. Previous MRI studies have shown age-related anatomical changes in gray matter, including a linear decrease in global gray matter volume (GMV) and regional GMV during aging [62]. As a result, using GMV as an input feature for estimating brain age not only presents its biological

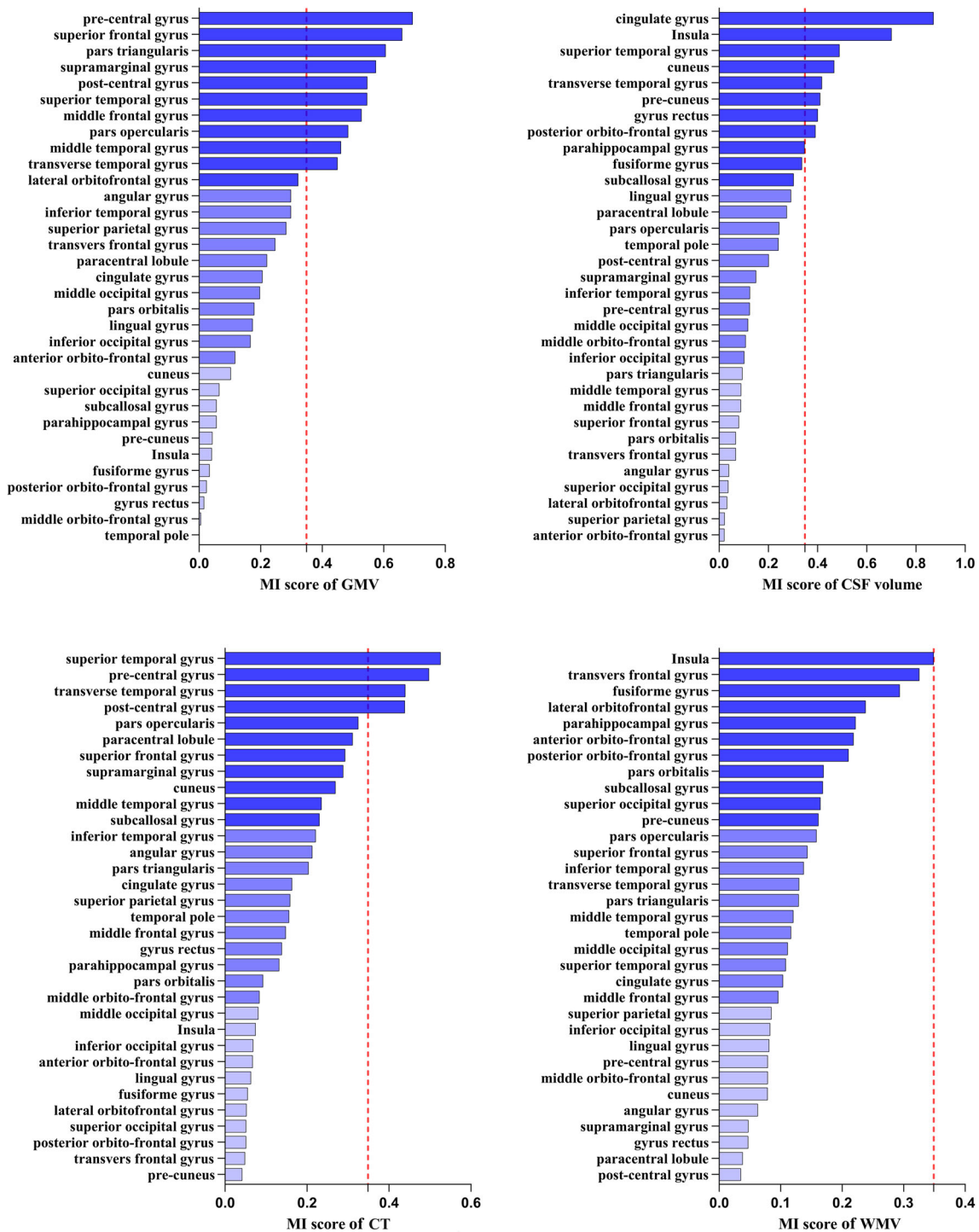


Fig. 2 Detailed ranking of mutual information (MI) value between estimated brain age after age-bias correction and four brain morphometric features (GMV, CSF volume, CT, and WMV) across 33 brain regions. Brain regions are classified into three groups based on MI values: the highest one-third, the middle one-third, and the lowest one-third depicted by varying color intensities. A red reference line is provided, indicating an MI value of 0.35, which is the MI between WMV in the insula and estimated brain age after age-bias correction. GMV, gray matter volume; CSF, cerebrospinal fluid; CT, cortical thickness; WMV, white matter volume

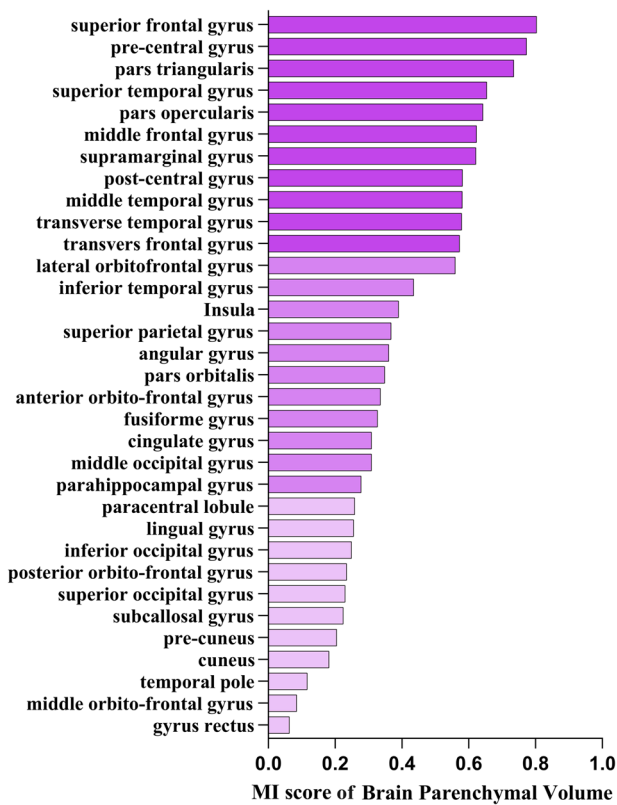


Fig. 3 Detailed ranking of mutual information (MI) values between estimated brain age after age-bias correction and brain parenchymal (GMV combined with WMV) features across 33 brain regions. The brain regions are classified into three groups based on MI values: the highest one-third, the middle one-third, and the lowest one-third depicted by varying color intensities

plausibility but also makes a substantial contribution to model performance. Additionally, another volumetric feature related to CSF volume exhibited the second-highest correlation coefficient with estimated brain age, following GMV. In line with a previous study [63], this finding also highlights the potential of CSF volume as a valuable feature for brain age estimation. Changes in CSF volume encapsulate information pertinent to brain age. However, it is important to note that the application of CSF-specific features in current studies of brain age remains limited. Second, among the features of brain parenchymal volume, the superior frontal gyrus (SFG) exhibited the strongest association with estimated brain age. From a perspective of neuroanatomy, the SFG is a prominent ridge located on the neocortex, constituting roughly one-third of the frontal lobe. From a perspective of neuropsychology, the core cognitive abilities thought to be dependent on the frontal cortex, such as task-switching, executive functions, verbal fluency, complex attention, and performance monitoring, are particularly

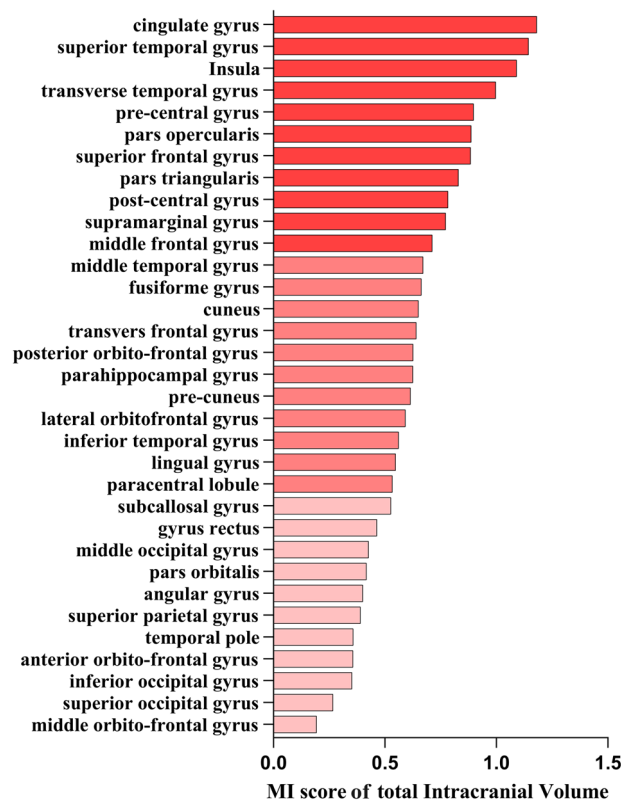


Fig. 4 Detailed ranking of mutual information (MI) between estimated brain age after age-bias correction and total intracranial volume (GMV combined with WMV and CSF volume) features across 33 brain regions. These brain regions are classified into three groups based on MI values: the highest one-third, the middle one-third, and the lowest one-third, visually represented by differences in color intensity

vulnerable to the aging process [64–67]. The linkage between neuroanatomy and cognitive functions may offer another unique perspective to understand the feature-specific brain age model. For instance, in 1997, Hannien et al discovered a positive correlation between category verbal fluency test (CVFT) scores and the volume of the frontal lobe [68]. Subsequently, Lu and her colleagues found that neurocognitive impairment (NCD) patients showing older brain age performed significantly worse on CVFT compared to normal aging controls [69]. Thus, our findings might confirm the significance of frontal volume in brain age estimation. When considering brain parenchymal and CSF volume, the total intracranial volume of the cingulate had the highest MI value with brain age, which may highlight the significance of the cingulate gyrus in age-related brain changes. In Alzheimer’s disease (AD), MRI studies consistently report reduced volumes of the cingulate gyrus compared to normal controls [70, 71], with voxel-based morphometric analysis indicating decreased gray matter density, particularly in the posterior regions [72–74]. Reduced metabolic changes (i.e.,

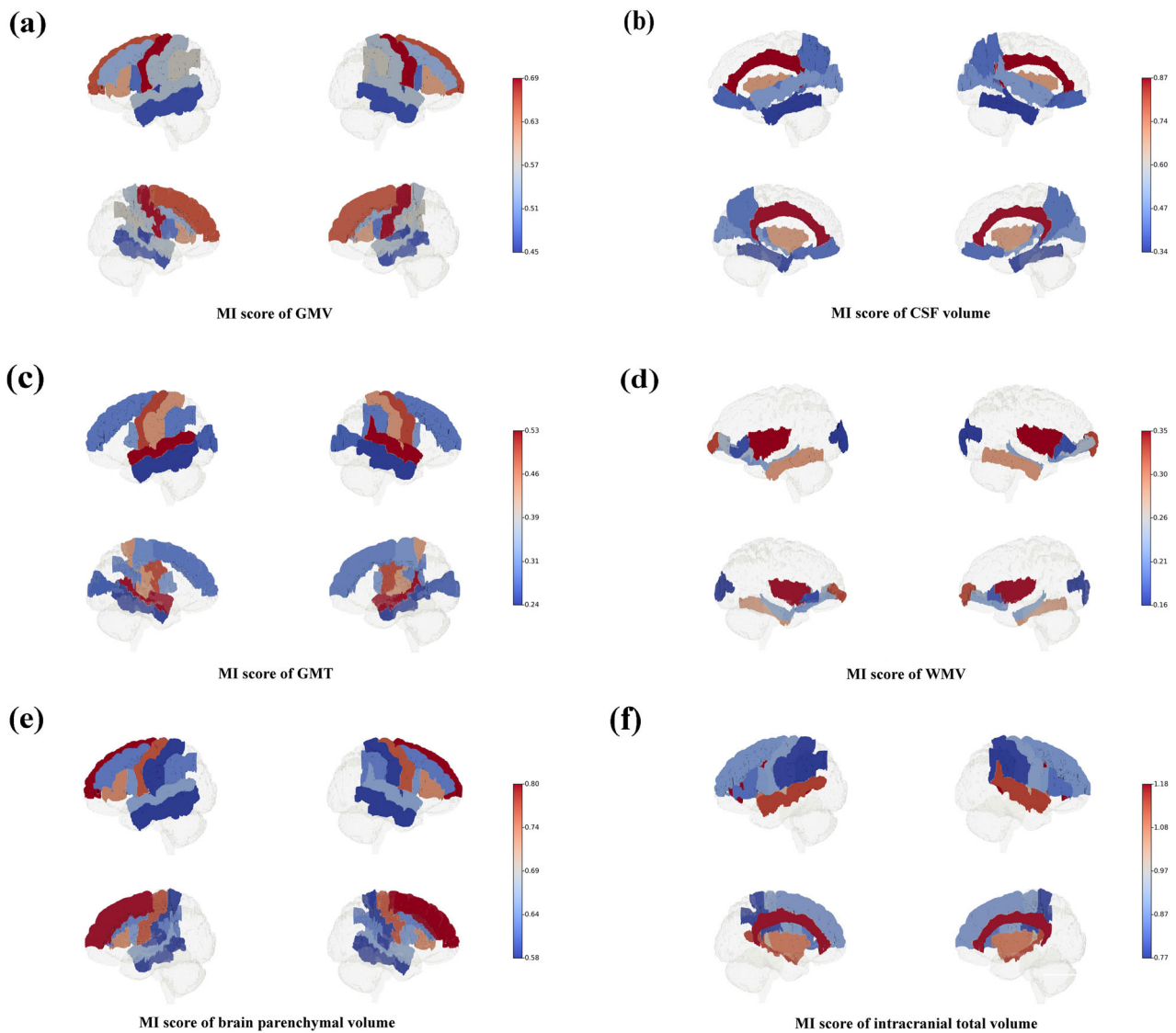


Fig. 5 This figure illustrates brain heatmaps showcasing the top ten brain regions in the BCI-DNI atlas, ranked by mutual information (MI) values. **a** shows the top ten regions in gray matter volume (GMV). The pre-central gyrus demonstrates the highest MI value (0.69). **b** illustrates the top ten regions in cerebrospinal fluid (CSF) volume. The cingulate exhibits the highest MI value (0.87). **c** displays the top ten regions in cortical thickness. The superior temporal gyrus exhibits the highest MI value (0.53). **d** presents the top ten regions in white matter volume (WMV). The insula shows the highest MI value (0.35). **e** depicts the top ten regions in brain parenchyma volume (combining GMV and WMV). The superior frontal gyrus displays the highest MI value (0.80) among brain regions. **f** shows the top ten regions in intracranial total volume (the combination of GMV, WMV, and CSF volume). The cingulate showed the highest total MI value (1.18)

hypometabolism) in the posterior cingulate gyrus have also been observed in AD patients using magnetic resonance spectroscopy [75] and and positron emission tomography [76–78]. Understanding the changes in the cingulate might help to address cognitive decline in aging and neurodegenerative diseases and further tailor the preventive measures for brain health.

The findings of this study mark a significant and practical advancement for several reasons. First, we

incorporated four distinct morphometric features into the brain age model simultaneously, taking a whole-brain perspective. In the field of brain age research, raw MRI scans are commonly used as input features due to their inherent multidimensional morphometric information [54, 79–81]. We improved the interpretability of brain age models by extracting regional morphometric information from MRI scans through quantitative pre-processing, which was utilized as input features. Second, this study

explored a novel use of MI as a standardized method to interpret brain age models. MI is an ideal statistic for quantifying the degree of relationship between variables in multiple ways [82]. The rates of brain atrophy vary nonlinearly with age, as observed in the temporal lobe [83] while showing a linear pattern in regions such as the hippocampus and frontal lobe [84, 85]. MI could equally quantify the correlation between each brain region feature and brain age at the individual level. Besides, the nonlinear nature of the relationship between regional morphometric features and brain age may explain why multivariate linear regression models often lack optimal performance in brain age studies. In contrast, support vector machine (SVM), as a commonly used computational model, can effectively capture both linear and nonlinear relationships [45, 86]. Besides, MI provides a straightforward interpretation by measuring the shared information between morphometric features and estimated brain age, grounded on the well-established theoretical framework of information theory. With an advantage of independence, MI is insensitive to the size of the datasets and thus, can converge with tight error bounds to a measure of relatedness [29].

Although our model showed slight overfitting in the testing set, we deliberately avoided using the techniques of dimensionality reduction, such as principal component analysis, or independent component analysis for pre-processing. We retained all the input features during training and testing to maintain the interpretability of brain age estimation and avoid the obfuscation introduced by the techniques of dimensionality reduction. Our objective was to evaluate the interpretability of regional-level features for brain age predictions in an independent testing set rather than pursuing lower MAE. Still, our model's accuracy is comparable to that of other brain age studies [8, 21].

Conclusion

Using the mutual information between morphometric features and estimated brain age is a promising way to assess the regional contributions to brain age. The significant roles of frontal gray matter volume and limbic CSF volume highlight that regional gray matter and CSF are key features that determine the estimated brain age, which may add value to existing computational models of brain age.

Limitations and future directions

The findings of this study have to be interpreted in the context of limitations. First, we used two databases as the training and testing sets, which may limit the generalizability of our results. In future studies, our goal is to incorporate broader demographic databases with larger sample sizes to enhance the robustness of our findings. Second, our brain age model exhibited mild overfitting. We will improve the

prediction accuracy and generalization of the pre-trained model while retaining the dimensionality of input features, by increasing the data amount and exploring diverse regression models. Third, our analysis of brain morphometric features was limited to cortical regions. Additionally, we only utilized morphometric features extracted from a single modality of MRI (i.e., structure MRI) as training features in the brain age model. Incorporating multimodal age-related neuroimaging features, such as DTI-based (diffusion tensor imaging) metrics, white matter hyperintensities on T2-weighted MRI, as well as the presence and volume of metals on susceptibility-weighted imaging scans, could provide important supplementary information to the brain age prediction model, thereby enhancing the prediction efficiency of the trained algorithm. Lastly, fine-grained regional brain parcellation is essential for precision targeted therapy. We intend to refine brain parcellation, which will contribute to a more comprehensive analysis and interpretation of brain age in various neurological disorders.

Abbreviations

AD	Alzheimer's disease
Brain-PAD	Brain-predicted age difference
Cam-CAN	Cambridge Centre for Aging and Neuroscience
CSF	Cerebrospinal fluid
CT	Cortical thickness
CVFT	Category verbal fluency test
DL	Deep learning
GMV	Gray matter volume
MAE	Mean absolute error
MI	Mutual information
ML	Machine learning
RMSE	Root-mean-square error
SFG	Superior frontal gyrus
SVR	Support vector regression
WMV	White matter volume

Acknowledgements

The authors would like to thank the principal investigators of the Cam-CAN and brain development project. The funders were not involved in the study design, data collection and analysis, or the preparation of the article.

Authors contributions

J.L. and H.L. were responsible for conceptualizing the study, performing the morphometric analyses, and preparing the manuscript. J.L. assisted in calculating the brain age models and organizing the results. The research teams of Cam-CAN and the brain development project provided the imaging data. J.L., H.L. and L.C.W. were involved in data interpretation. All the authors reviewed the manuscript and approved the final manuscript.

Funding

This work was supported by the Hong Kong Research Grant Council (RGC)-General Research Fund (GRF) (Grant No. 14111021) and Healthy Longevity Catalyst Awards (Hong Kong) (Project No. HLCA/M-407/23). The corresponding author had full access to all of the data in the study and had final responsibility for the decision to submit for publication.

Data availability

The data supporting the findings of this study are available on request from the corresponding author. The data are not publicly available due to privacy or ethical restrictions.

Declarations

Ethics approval and consent to participate

For the purpose of this study, we used the structural MRI scans of Cam-CAN that were previously collected under the study protocols at the University of Cambridge. This study was carried out in accordance with the recommendations of the University's Institutional Review Board (IRB). The protocol was approved by the University's IRB. All participants were given written informed consent at the time of study participation. All participants gave written informed consent in accordance with the Declaration of Helsinki. The University's IRB also provided explicit approval for open sharing of the anonymized data. The current study was approved by the Clinical Research Ethics Committee of The Chinese University of Hong Kong (CUHK) and New Territories East Cluster (NTEC) (The Joint CUHK-NTEC) (Ref No. 2023.496).

Consent for publication

Not applicable.

Competing interests

All authors declare no competing interests.

Received: 12 April 2024 Accepted: 31 July 2024

Published online: 26 August 2024

References

- Davies N (2011) Promoting healthy ageing: the importance of lifestyle. *Nurs Stand* 25:43–49
- Burke SN, Barnes CA (2006) Neural plasticity in the ageing brain. *Nat Rev Neurosci* 7:30–40
- Morrison JH, Baxter MG (2012) The ageing cortical synapse: hallmarks and implications for cognitive decline. *Nat Rev Neurosci* 13:240–250
- Sullivan EV, Pfefferbaum A (2007) Neuroradiological characterization of normal adult ageing. *Br J Radiol* 80:S99–S108
- Podgórski P, Bładowska J, Sasiadek M (2021) Novel volumetric and surface-based magnetic resonance indices of the aging brain—does male and female brain age in the same way? *Front Neurol* 12:645729
- Franke K, Ziegler G, Klöppel S, Gaser C, Alzheimer's Disease Neuroimaging Initiative (2010) Estimating the age of healthy subjects from T1-weighted MRI scans using kernel methods: exploring the influence of various parameters. *Neuroimage* 50:883–892
- Cole JH, Franke K (2017) Predicting age using neuroimaging: innovative brain ageing biomarkers. *Trends Neurosci* 40:681–690
- Franke K, Gaser C (2019) Ten years of BrainAGE as a neuroimaging biomarker of brain aging: what insights have we gained? *Front Neurol* 10:454252
- Cole JH, Underwood J, Caan MWA et al (2017) Increased brain-predicted aging in treated HIV disease. *Neurology* 88:1349–1357
- Nenadić I, Dietzek M, Langbein K, Sauer H, Gaser C (2017) BrainAGE score indicates accelerated brain aging in schizophrenia, but not bipolar disorder. *Psychiatry Res Neuroimaging* 266:86–89
- Koutsouleris N, Davatzikos C, Borgwardt S et al (2014) Accelerated brain aging in schizophrenia and beyond: a neuroanatomical marker of psychiatric disorders. *Schizophr Bull* 40:1140–1153
- Franke K, Gaser C (2012) Longitudinal changes in individual BrainAGE in healthy aging, mild cognitive impairment, and Alzheimer's disease. *GeroPsych* 25:235–245
- Gaser C, Franke K, Klöppel S, Koutsouleris N, Sauer H, Alzheimer's Disease Neuroimaging Initiative (2013) BrainAGE in mild cognitive impaired patients: predicting the conversion to Alzheimer's disease. *PLoS One* 8:e67346
- Löwe LC, Gaser C, Franke K, Alzheimer's Disease Neuroimaging Initiative (2016) The effect of the APOE genotype on individual BrainAGE in normal aging, mild cognitive impairment, and Alzheimer's disease. *PLoS One* 11:e0157514
- Biondo F, Jewell A, Pritchard M et al (2022) Brain-age is associated with progression to dementia in memory clinic patients. *Neuroimage Clin* 36:103175
- Franke K, Luders E, May A, Wilke M, Gaser C (2012) Brain maturation: predicting individual BrainAGE in children and adolescents using structural MRI. *Neuroimage* 63:1305–1312
- Raz N, Ghisletta P, Rodrigue KM, Kennedy KM, Lindenberger U (2010) Trajectories of brain aging in middle-aged and older adults: regional and individual differences. *Neuroimage* 51:501–511
- Storsve AB, Fjell AM, Tamnes CK et al (2014) Differential longitudinal changes in cortical thickness, surface area and volume across the adult life span: regions of accelerating and decelerating change. *J Neurosci* 34:8488–8498
- Fjell AM, Westlye LT, Grydeland H et al (2013) Critical ages in the life course of the adult brain: nonlinear subcortical aging. *Neurobiol Aging* 34:2239–2247
- Baecker L, Dafflon J, Da Costa PF et al (2021) Brain age prediction: a comparison between machine learning models using region- and voxel-based morphometric data. *Hum Brain Mapp* 42:2332–2346
- Massett RJ, Maher AS, Imms PE et al (2023) Regional neuroanatomic effects on brain age inferred using magnetic resonance imaging and ridge regression. *J Gerontol A Biol Sci Med Sci* 78:872–881
- Lee WH, Antoniadou M, Schnack HG, Kahn RS, Frangou S (2021) Brain age prediction in schizophrenia: does the choice of machine learning algorithm matter? *Psychiatry Res Neuroimaging* 310:111270
- Da Costa PF, Dafflon J, Pinaya WHL (2020) Brain-age prediction using shallow machine learning: predictive analytics competition 2019. *Front Psychiatry* 11:604478
- More S, Antonopoulos G, Hoffstaedter F et al (2023) Brain-age prediction: a systematic comparison of machine learning workflows. *Neuroimage* 270:119947
- Darıcı MB, Yıldırım Ş, Gezer M (2021) Brain age estimation from MRI images using 2D-CNN instead of 3D-CNN. *Acta Inf* 5:373–385
- Watson DS, Krutzinna J, Bruce IN et al (2019) Clinical applications of machine learning algorithms: beyond the black box. *BMJ* 364:l886
- Kraskov A, Stögbauer H, Grassberger P (2004) Estimating mutual information. *Phys Rev E* 69:066138
- Slonim N, Atwal GS, Tkacik G, Bialek W (2005) Estimating mutual information and multi-information in large networks. *arXiv preprint cs/0502017*
- Ross BC (2014) Mutual information between discrete and continuous data sets. *PLoS One* 9:e87357
- Shafto MA, Tyler LK, Dixon M et al (2014) The Cambridge Centre for Ageing and Neuroscience (Cam-CAN) study protocol: a cross-sectional, lifespan, multidisciplinary examination of healthy cognitive ageing. *BMC Neurol* 14:1–25
- Shattuck DW, Leahy RM (2002) BrainSuite: an automated cortical surface identification tool. *Med Image Anal* 6:129–142
- Apostolova LG, Thompson PM, Rogers SA et al (2010) Surface feature-guided mapping of cerebral metabolic changes in cognitively normal and mildly impaired elderly. *Mol Imaging Biol* 12:218–224
- Lu H, Ma SL, Chan SSM, Lam LCW (2016) The effects of apolipoprotein ε 4 on aging brain in cognitively normal Chinese elderly: a surface-based morphometry study. *Int Psychogeriatr* 28:1503–1511
- Geric G, Kubler O, Kikinis R, Jolesz FA (1992) Nonlinear anisotropic filtering of MRI data. *IEEE Trans Med Imaging* 11:221–232
- Marr D, Hildreth E (1980) Theory of edge detection. *Proc R Soc Lond Ser B Biol Sci* 207:187–217
- Sandor S, Leahy R (1997) Surface-based labeling of cortical anatomy using a deformable atlas. *IEEE Trans Med Imaging* 16:41–54
- Joshi AA, Choi S, Liu Y et al (2022) A hybrid high-resolution anatomical MRI atlas with sub-parcellation of cortical gyri using resting fMRI. *J Neurosci Methods* 374:109566
- Geschwind N, Levitsky W (1968) Human brain: left-right asymmetries in temporal speech region. *Science* 161:186–187
- Toga AW, Thompson PM (2003) Mapping brain asymmetry. *Nat Rev Neurosci* 4:37–48
- Duboc V, Dufourcq P, Blader P, Roussigné M (2015) Asymmetry of the brain: development and implications. *Annu Rev Genet* 49:647–672
- Le TT, Kuplicki RT, McKinney BA et al (2018) A nonlinear simulation framework supports adjusting for age when analyzing BrainAGE. *Front Aging Neurosci* 10:317
- Niu X, Zhang F, Kounios J, Liang H (2020) Improved prediction of brain age using multimodal neuroimaging data. *Hum Brain Mapp* 41:1626–1643

43. Le TT, Kuplicki R, Yeh HW et al (2018) Effect of ibuprofen on BrainAGE: a randomized, placebo-controlled, dose-response exploratory study. *Biol Psychiatry Cogn Neurosci Neuroimaging* 3:836–843
44. Ganaie MA, Tanveer M, Beheshti I (2024) Brain age prediction using improved twin SVR. *Neural Comput Appl* 36:53–63
45. Drucker H, Burges CJ, Kaufman L, Smola A, Vapnik V (1996) Support vector regression machines. *Adv Neural Inf Process Syst* 9:155–161
46. Pedregosa F, Varoquaux G, Gramfort A et al (2011) Scikit-learn: machine learning in Python. *J Mach Learn Res* 12:2825–2830
47. Hastie T, Tibshirani R, Friedman JH (2009) The elements of statistical learning: data mining, inference, and prediction. Springer, New York
48. Smith SM, Vidaurre D, Alfaro-Almagro F, Nichols TE, Miller KL (2019) Estimation of brain age delta from brain imaging. *Neuroimage* 200:528–539
49. Treder MS, Shock JP, Stein DJ, Du Plessis S, Seedat S, Tsvetanov KA (2021) Correlation constraints for regression models: controlling bias in brain age prediction. *Front Psychiatry* 12:615754
50. Beheshti I, Nugent S, Potvin O, Duchesne S (2019) Bias-adjustment in neuroimaging-based brain age frameworks: a robust scheme. *Neuroimage Clin* 24:102063
51. Shannon CE (1948) A mathematical theory of communication. *Bell Syst Tech J* 27:379–423
52. Chai T, Draxler RR (2014) Root mean square error (RMSE) or mean absolute error (MAE). *Geosci Model Dev Discuss* 7:1525–1534
53. Di Buccianico A (2008) Coefficient of determination (R^2). In: *Encyclopedia of Statistics in Quality and Reliability*. Hoboken: Wiley. 1
54. Cole JH, Poudel RP, Tsagkrasoulis D et al (2017) Predicting brain age with deep learning from raw imaging data results in a reliable and heritable biomarker. *Neuroimage* 163:115–124
55. Monté-Rubio GC, Falcón C, Pomarol-Clotet E, Ashburner J (2018) A comparison of various MRI feature types for characterizing whole brain anatomical differences using linear pattern recognition methods. *Neuroimage* 178:753–768
56. Wang J, Knol MJ, Tiulpin A et al (2019) Gray matter age prediction as a biomarker for risk of dementia. *Proc Natl Acad Sci U S A* 116:21213–21218
57. Ballester PL, Suh JS, Ho NCW et al (2023) Gray matter volume drives the brain age gap in schizophrenia: a SHAP study. *Schizophrenia* 9:3
58. Sun J, Tu Z, Meng D, Gong Y, Zhang M, Xu J (2022) Interpretation for individual brain age prediction based on gray matter volume. *Brain Sci* 12:1517
59. Steffener J, Habeck C, O'Shea D, Razlighi Q, Bherer L, Stern Y (2016) Differences between chronological and brain age are related to education and self-reported physical activity. *Neurobiol Aging* 40:138–144
60. Adluru N, Korponay CH, Norton DL, Goldman RI, Davidson RJ (2020) BrainAGE and regional volumetric analysis of a Buddhist monk: a longitudinal MRI case study. *Neurocase* 26:79–90
61. Karim HT, Ly M, Yu G et al (2021) Aging faster: worry and rumination in late life are associated with greater brain age. *Neurobiol Aging* 101:13–21
62. Good CD, Johnsrude IS, Ashburner J, Henson RN, Friston KJ, Frackowiak RS (2001) A voxel-based morphometric study of ageing in 465 normal adult human brains. *Neuroimage* 14:21–36
63. Cole JH, Ritchie SJ, Bastin ME et al (2018) Brain age predicts mortality. *Mol Psychiatry* 23:1385–1392
64. Chao LL, Knight RT (1997) Prefrontal deficits in attention and inhibitory control with aging. *Cereb Cortex* 7:63–69
65. Craik FI, Grady CL (2002) Aging, memory, and frontal lobe functioning. In: *Principles of frontal lobe function* (Stuss DT, Knight RT, eds), pp. 528–540. London: Oxford University Press
66. MacLulich AMJ, Ferguson KJ, Deary IJ, Seckl JR, Starr JM, Wardlaw JM (2002) Intracranial capacity and brain volumes are associated with cognition in healthy elderly men. *Neurology* 59:169–174
67. Cannon T, Bilker W, Gur RE, Colwell P, Turetsky BI, Gallacher F (1998) A follow-up magnetic resonance imaging study of schizophrenia. *Arch Gen Psychiatry* 55:H5–H152
68. Hanninen T, Hallikainen M, Koivisto K et al (1997) Decline of frontal lobe functions in subjects with age-associated memory impairment. *Neurology* 48:148–153
69. Lu H, Li J, Fung AWT, Lam LCW (2023) Diversity in verbal fluency performance and its associations with MRI-informed brain age matrices in normal ageing and neurocognitive disorders. *CNS Neurosci Ther* 29:1865–1880
70. Callen DJA, Black SE, Gao F, Caldwell CB, Szalai JP (2001) Beyond the hippocampus: MRI volumetry confirms widespread limbic atrophy in AD. *Neurology* 57:1669–1674
71. Killiany RJ, Gomez-Isla T, Moss M et al (2000) Use of structural magnetic resonance imaging to predict who will get Alzheimer's disease. *Ann Neurol* 47:430–439
72. Baron JC, Chételat G, Desgranges B et al (2001) In vivo mapping of gray matter loss with voxel-based morphometry in mild Alzheimer's disease. *Neuroimage* 14:298–309
73. Frisoni GB, Testa C, Zorzan A et al (2002) Detection of grey matter loss in mild Alzheimer's disease with voxel based morphometry. *J Neurol Neurosurg Psychiatry* 73:657–664
74. Scahill RI, Schott JM, Stevens JM, Rossor MN, Fox NC (2002) Mapping the evolution of regional atrophy in Alzheimer's disease: unbiased analysis of fluid-registered serial MRI. *Proc Natl Acad Sci U S A* 99:4703–4707
75. Kizu O, Yamada K, Ito H, Nishimura T (2004) Posterior cingulate metabolic changes in frontotemporal lobar degeneration detected by magnetic resonance spectroscopy. *Neuroradiology* 46:277–281
76. Matsuda H, Kitayama N, Ohnishi T et al (2002) Longitudinal evaluation of both morphologic and functional changes in the same individuals with Alzheimer's disease. *J Nucl Med* 43:304–311
77. Minoshima S, Giordani B, Berent S, Frey KA, Foster NL, Kuhl DE (1997) Metabolic reduction in the posterior cingulate cortex in very early Alzheimer's disease. *Ann Neurol* 42:85–94
78. Valla J, Berndt JD, Gonzalez-Lima F (2001) Energy hypometabolism in posterior cingulate cortex of Alzheimer's patients: superficial laminar cytochrome oxidase associated with disease duration. *J Neurosci* 21:4923–4930
79. Fisch L, Ernsting J, Winter NR et al (2021) Predicting brain-age from raw T1-weighted magnetic resonance imaging data using 3D convolutional neural networks. *ArXiv Preprint ArXiv:2103.11695*
80. Wood DA, Kafabadi S, Al Busaidi A et al (2022) Accurate brain-age models for routine clinical MRI examinations. *Neuroimage* 249:118871
81. Hu L, Wan Q, Huang L et al (2023) MRI-based brain age prediction model for children under 3 years old using deep residual network. *Brain Struct Funct* 228:1771–1784
82. Cover TM (1999) *Elements of information theory*. John Wiley & Sons
83. Schuff N, Tosun D, Insel PS et al (2012) Nonlinear time course of brain volume loss in cognitively normal and impaired elders. *Neurobiol Aging* 33:845–855
84. Bartzokis G, Beckson M, Lu PH, Nuechterlein KH, Edwards N, Mintz J (2001) Age-related changes in frontal and temporal lobe volumes in men: a magnetic resonance imaging study. *Arch Gen Psychiatry* 58:461–465
85. Cohen RM, Szczepanik J, McManus M et al (2006) Hippocampal atrophy in the healthy is initially linear and independent of age. *Neurobiol Aging* 27:1385–1394
86. Awad M, Khanna R (2015) *Efficient learning machines: theories, concepts, and applications for engineers and system designers*. Springer nature, Basingstoke, UK

Publisher's Note

Springer Nature remains neutral with regard to jurisdictional claims in published maps and institutional affiliations.